

## Supplementary Information

### On the Formation of Hydrogen Peroxide in Water Microdroplets

Adair Gallo Jr.<sup>1,&</sup>, Nayara H. Musskopf<sup>1,&</sup>, Xinlei Liu<sup>2</sup>, Ziqiang Yang<sup>2</sup>, Jeferson Petry<sup>1</sup>, Peng Zhang<sup>1</sup>, Sigurdur Thoroddsen<sup>2</sup>, Hong Im<sup>2</sup>, Himanshu Mishra<sup>1,\*</sup>

<sup>1</sup>Interfacial Lab (iLab), Biological and Environmental Science and Engineering (BESE) Division, Water Desalination and Reuse Center (WDRC), King Abdullah University of Science and Technology (KAUST), Thuwal 23955-6900, Saudi Arabia

<sup>2</sup>Physical Science and Engineering (PSE) Division, King Abdullah University of Science and Technology (KAUST), Thuwal 23955-6900, Saudi Arabia

<sup>&</sup>Equal author contribution

\*[Himanshu.Mishra@kaust.edu.sa](mailto:Himanshu.Mishra@kaust.edu.sa)

SI Movie S1:

**Caption:** A representative high-speed video of pneumatic sprays formed in our concentric tubular geometry with high-speed external nitrogen gas flow (5.3 L/min) and a slower inner water jet (100  $\mu$ L/min). The video was recorded using a Kirana-05M camera at 5 million frames per second (fps); the 200 ns time-resolution of this platform enabled us to observe microdroplets trajectories before, during, and after their interaction with the shearing gas.

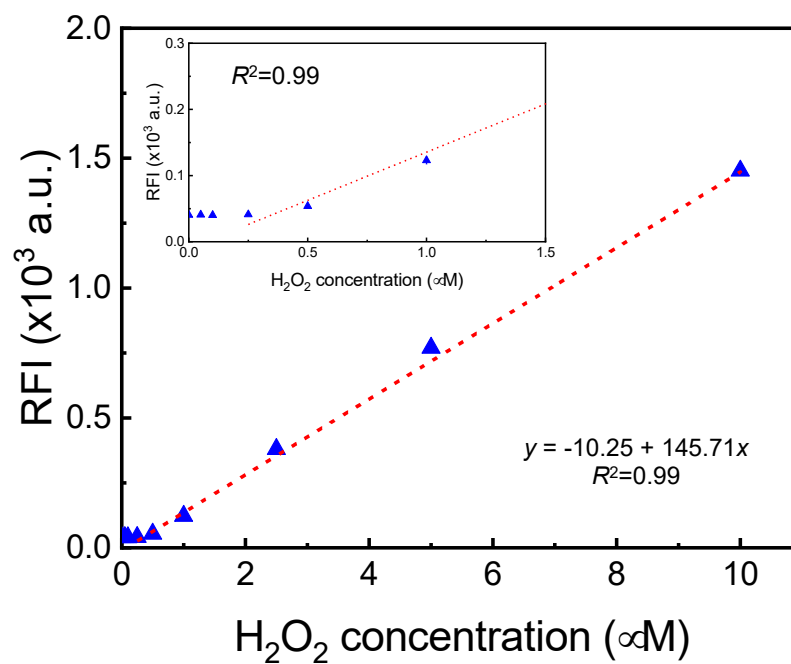


Fig. S1 – Calibration curve for H<sub>2</sub>O<sub>2</sub> concentration using the Hydrogen Peroxide Assay Kit (HPAK) with fluorescence maximum absorption and emission at 647 and 674 nm, respectively. It is identical with our previous report<sup>1</sup>.

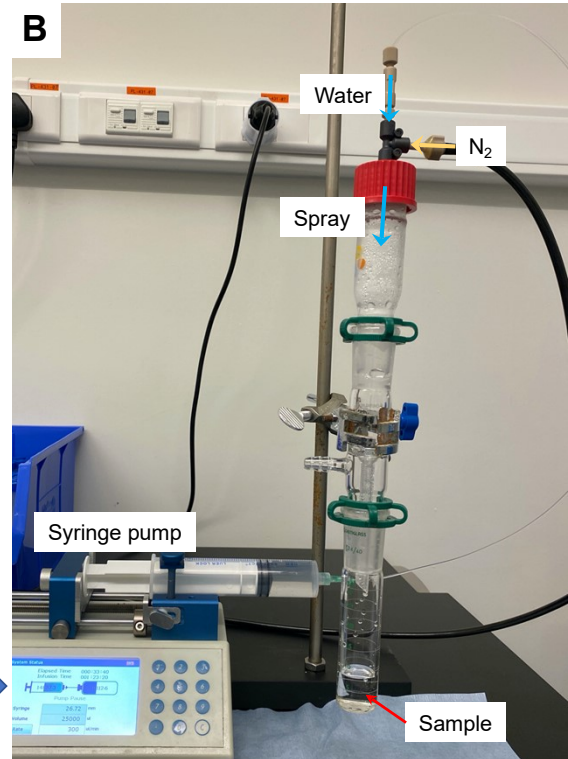
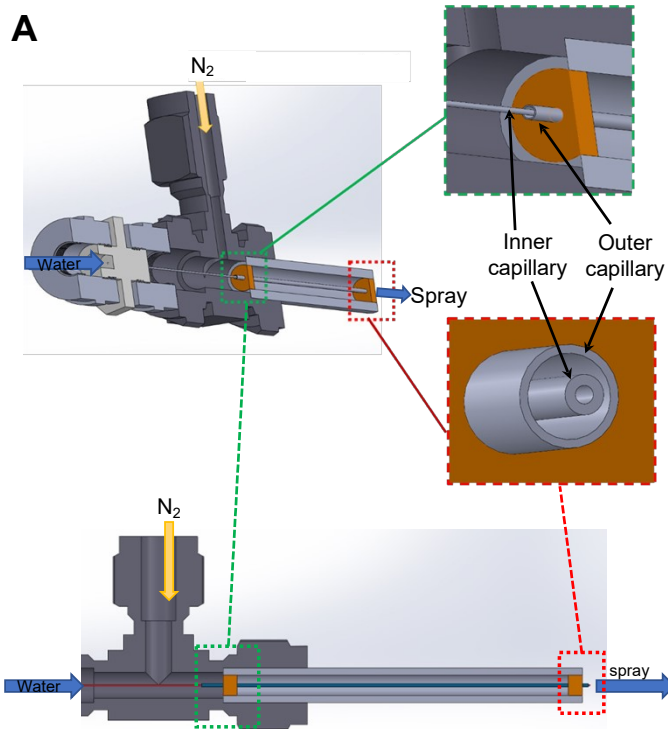


Fig. S2 – (A) Schematics of pneumatic spray setup. (B) Photograph of spray setup connected to a glass flask for sample collection.

Table S1 – Dimensions of a few models of our custom-built pneumatic spray setups

Spray type	Inner capillary ( $\pm 5 \mu\text{m}$ )		Outer capillary ( $\pm 5 \mu\text{m}$ )		Coaxial	N <sub>2</sub> flow cross-section
	Inner dia. ( $\mu\text{m}$ )	Outer dia. ( $\mu\text{m}$ )	Inner dia. ( $\mu\text{m}$ )	Outer dia. ( $\mu\text{m}$ )	Length ( $\pm 1 \text{ mm}$ )	Area ( $\mu\text{m}^2$ )
<b>Spray A (main)</b>	100	228	432	585	24	421663
Spray B	106	222	489	587	24	596554
Spray C	113	217	404	712	46	366282
Spray D	89	213	473	731	79	562181

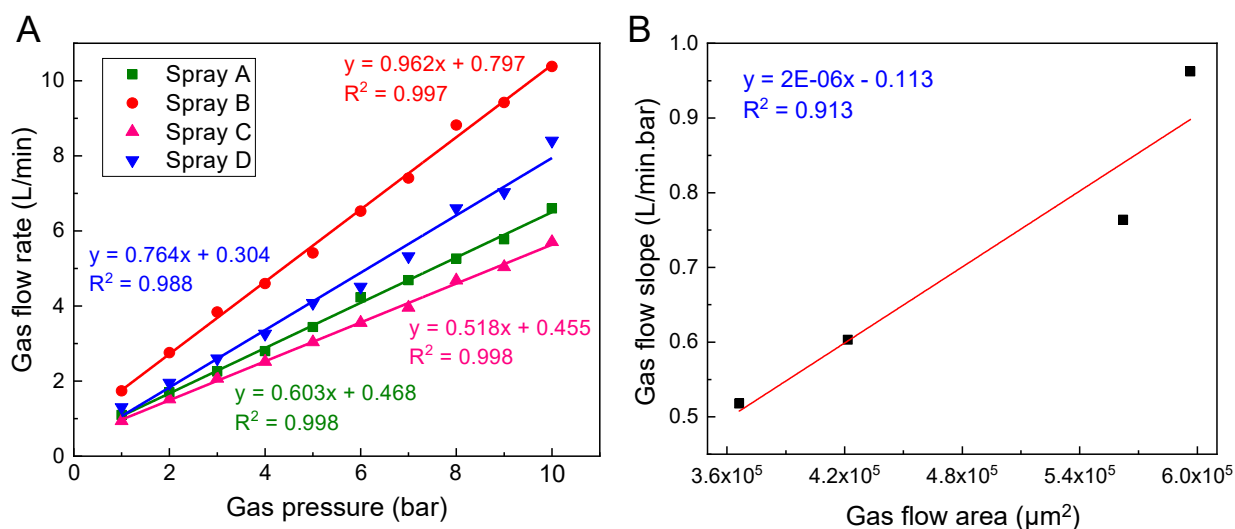


Fig. S3 – (A) Dependence of gas flow rate on in-line gas pressure for four different types of custom-built sprays, whose dimensions are shown in Table S1. (B) Linear correlation between the slopes of gas flow rate by in-line gas pressure (from A) and gas flow area of the four different sprays.

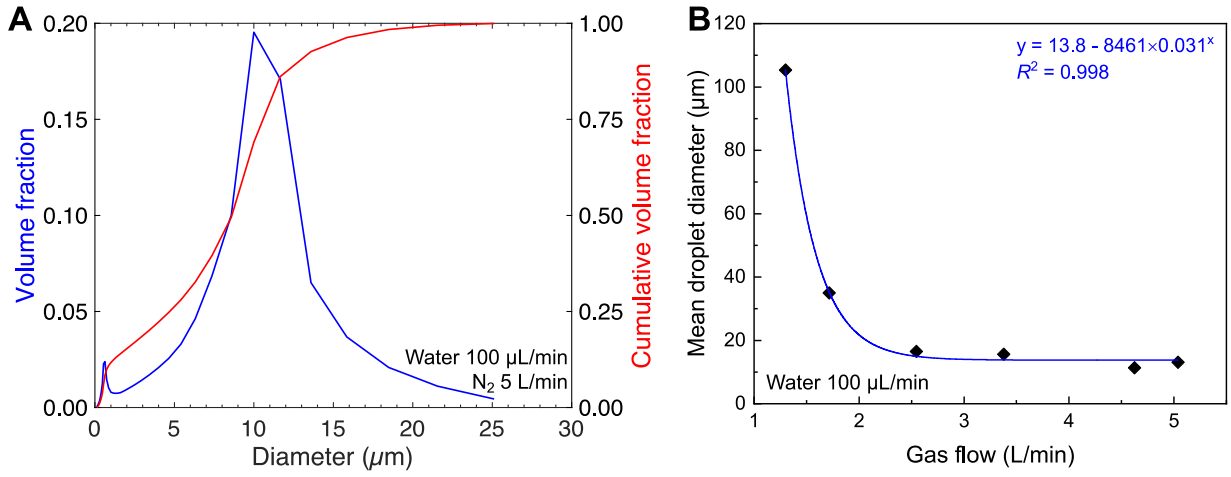


Fig. S4 – (A) Droplet size distribution and (B) droplet mean diameter as function of gas flowrate in sprays.

## Section S1. Theoretical and computational section

Before computational fluid dynamic (CFD) simulations, a theoretical calculation was conducted based on the Rankine-Hugoniot conditions, because from a CFD simulation point of view  $\text{H}_2\text{O}_2$  could only be generated by high-temperature reactions. To generate high temperatures, the shock wave is a possible approach. By using a high-speed  $\text{N}_2$  gas, the interaction between  $\text{N}_2$  and a relatively static water jet could lead to shock waves. In the experiment, a high-pressure (8.27 bar) co-flow  $\text{N}_2$  gas was employed. By using the momentum and energy conservation equations,

$$\rho_1 u_1^2 + p_1 = \rho_2 u_2^2 + p_2 \quad (1)$$

$$h_1 + u_1^2/2 = h_2 + u_2^2/2 \quad (2)$$

We know that the exit velocity of the high-speed gas is about 792 m/s at room temperature. When the high-speed gas hits the water droplet, almost all of the momentum energy is converted to heat. If we assume the heat capacity does not change. Then the temperature rise of the static gas is  $\frac{u_2^2}{2}/c_p$ , which is about 301 K. Schematic of the process is depicted in Fig. S5.

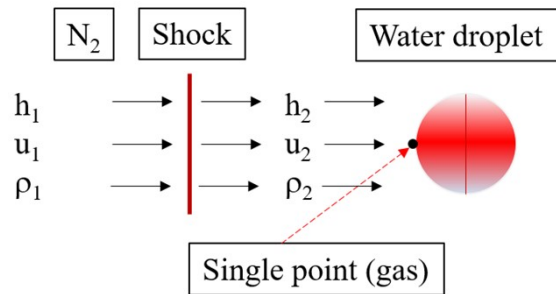


Fig. S5. Schematic of the interaction between high-pressure  $\text{N}_2$  gas and static water droplet.

To further clarify the gas-water interaction process, three-dimensional (3D) CFD simulations were performed using the Converge code. The turbulence is simulated by the renormalization group  $k-\varepsilon$  model<sup>2</sup>. The Eulerian void of fluid (VOF) method<sup>3</sup> was adopted to capture the in- and near-nozzle spray details. In this method, the gas and liquid fuel are considered as a single compressible fluid mixture, and the void fraction ( $\alpha_l$ ) is used to represent the volume fraction of liquid. Details of the related models are available in<sup>4</sup>. Fig. S6 illustrates the computational domain (200  $\mu\text{m}$  in diameter and 400  $\mu\text{m}$  in length). To mimic the experiment, the inlet boundary was imposed with a high-speed  $\text{N}_2$  gas was imposed and three droplets with a

diameter of 20  $\mu\text{m}$  were scattered in the central domain. A base mesh size of 5  $\mu\text{m}$  was used and a fixed embedding region was adopted with a refined scale of 4, which yields a minimum mesh size of 0.625  $\mu\text{m}$ . A varying time step was used by controlling the convective Courant flow number to be below 0.5.

Fig. 3 shows the predicted distributions of pressure and temperature flow fields at 0.1  $\mu\text{s}$ . Note that the pressure jumps to a significantly high level when the high-speed gas impinges onto the static water droplet, which results in a high-temperature rise of about 300 K, in agreement with the theoretic calculation.

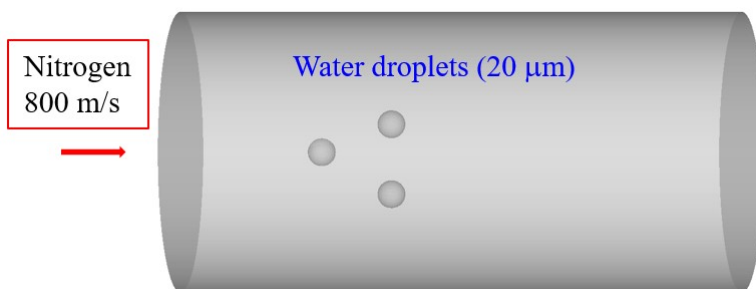


Fig. S6. Schematic of the computational domain.

However, a 300 K temperature rise might not be enough to explain the significant growth of  $\text{H}_2\text{O}_2$  production during the experiment. Further zero-dimensional simulations were conducted to evaluate the effects of temperature on  $\text{H}_2\text{O}_2$  <sup>5</sup> formation using the SENKIN code. In simulations, a homogeneous constant volume reactor was employed with pure gas water as the single reactant. The boundary was at constant pressure (1 atm) and temperature conditions. Various temperatures and mixture residence times were studied and the final  $\text{H}_2\text{O}_2$  production was extracted for further analyses. Fig. S7 shows the predicted  $\text{H}_2\text{O}_2$  concentration at various temperatures and residence times. Expectedly, almost no  $\text{H}_2\text{O}_2$  was generated at low temperatures and residence times; a relatively high concentration of  $\text{H}_2\text{O}_2$  was generated only with a temperature over 1000 K and a residence time over 10  $\mu\text{s}$ . However, it should be noted that the concentration is only at an order of  $10^{-11}$  even at a high temperature and a long residence time.

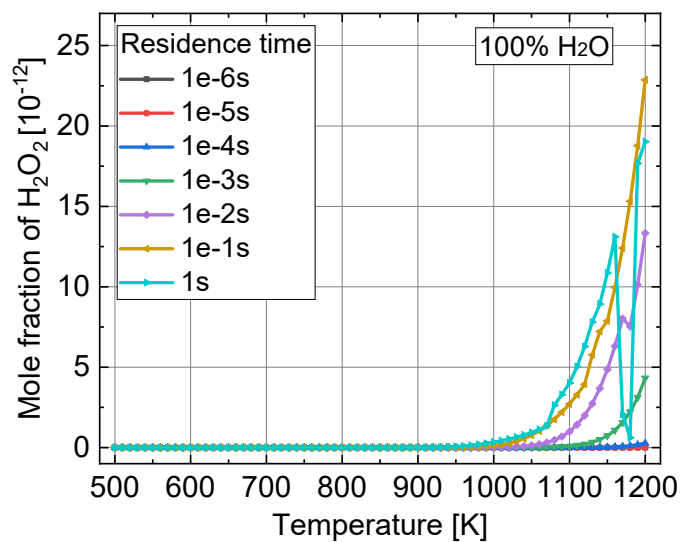


Fig. S7. Predicted H<sub>2</sub>O<sub>2</sub> concentration at various temperatures and residence times.

From the above results, it is assumed that a significant yield of H<sub>2</sub>O<sub>2</sub> is possible only at a high-temperature condition. However, based on the current shock wave and chemical reaction analyses, it is not possible to explain the observed formation of H<sub>2</sub>O<sub>2</sub> in the water microdroplets.

## Section S2. Glovebox experiments in the presence of ozone – rationale and details

The spray and condensation experiments were set up quite differently vis-à-vis the exposure to  $O_3(g)$ . The sprays were exposed to stable levels of ozone throughout the sample collection. This was realized by continuously supplying  $O_3(g)$  to the glovebox to maintain its partial pressure. In contrast, in the condensation experiments were initiated in the presence of  $O_3(g)$ , but it was no longer supplied during sample collection; so,  $O_3(g)$  depleted over time (Fig S8). The reasons behind the different methodologies are explained below.

Our spray setup was constantly injecting nitrogen into the glovebox at a 2.3 L/min flow rate. This nitrogen flowrate would rapidly dilute the  $O_3(g)$  in the glovebox, if we did not continuously add more  $O_3(g)$ . So, the partial pressure of  $O_3(g)$  in the glovebox was continuously adjusted by manually controlling the inflows of ozone, pure nitrogen and clean air. For instance, if the ozone level was increasing above a certain range (Fig S8C), the nitrogen (not the shearing gas of the spray) and air flows were increased for dilution. Thus, the glovebox inlet flows were: (i) ozone (+ air), (ii) nitrogen inflow from the spray, (iii) nitrogen for dilution, and (iv) air for dilution; and there was an outlet one-way valve to let gases escape. The ozone generator, rated for 24 g- $O_3$ /h production, was placed inside a sealed container with only an air inlet and air + ozone outlet. Since this setup generated an excessive ozone concentration in the outflow, way above the ppb levels we needed in this study, the air + ozone flow was split into two flows – one that was fed into the glovebox and another that was discarded to the fume hood. Additionally, since the dilutant air and nitrogen flows had significantly low relative humidities, the final RH in the glovebox varied in the range of 30%–70%.

Unlike the sprays, the condensation experiments, required relatively higher humidity to aid condensation on the cooled silicon wafers within a reasonable time. However, the dilutant air and nitrogen flows (used in the spray experiments) had a much lower humidity than required for condensation. Consequently, it was impractical to simultaneously control ozone and humidity levels in the glovebox by continuously adjusting all the gas inflows (mentioned above) and the heating rates of the water beaker or the ultrasonic humidifier power. Therefore, for the condensation experiments, we adjusted the concentration of ozone in the glovebox, then we closed all inflows of gases and placed the silicon wafers on top of ice bags to begin the condensation; the ozone concentration was then measured over the total period of condensation. It took about 40 minutes to collect adequate amount of condensate generated from the vapor supplied by humidifier

or heated water (40 °C) for the HPAK analysis for H<sub>2</sub>O<sub>2</sub>. During this period, the O<sub>3</sub>(g) concentration in the gas phase gradually decreased; in some cases, to levels below the detection limit (Fig. S8A-B).

For the condensation experiments, we present the final H<sub>2</sub>O<sub>2</sub> concentration in the condensates against the initial O<sub>3</sub>(g) concentration in Fig. 5 (green squares and red circles); while for the spray experiments Fig. 5 (blue triangles), we present the final H<sub>2</sub>O<sub>2</sub> concentration in the collected sample against the mean O<sub>3</sub>(g) concentration during the 5 minutes of spray collection. Here, it must be recognized that the system never attained thermodynamic equilibrium, nor was it intended to. Additionally, a number of factors influenced the fate of O<sub>3</sub>(g), for instance, it reacted with and/or adsorbed onto surfaces inside of the glovebox such as the frame, nuts/bolts, electrical outlets, etc.; some O<sub>3</sub> also leaked through the outlet of the glovebox.

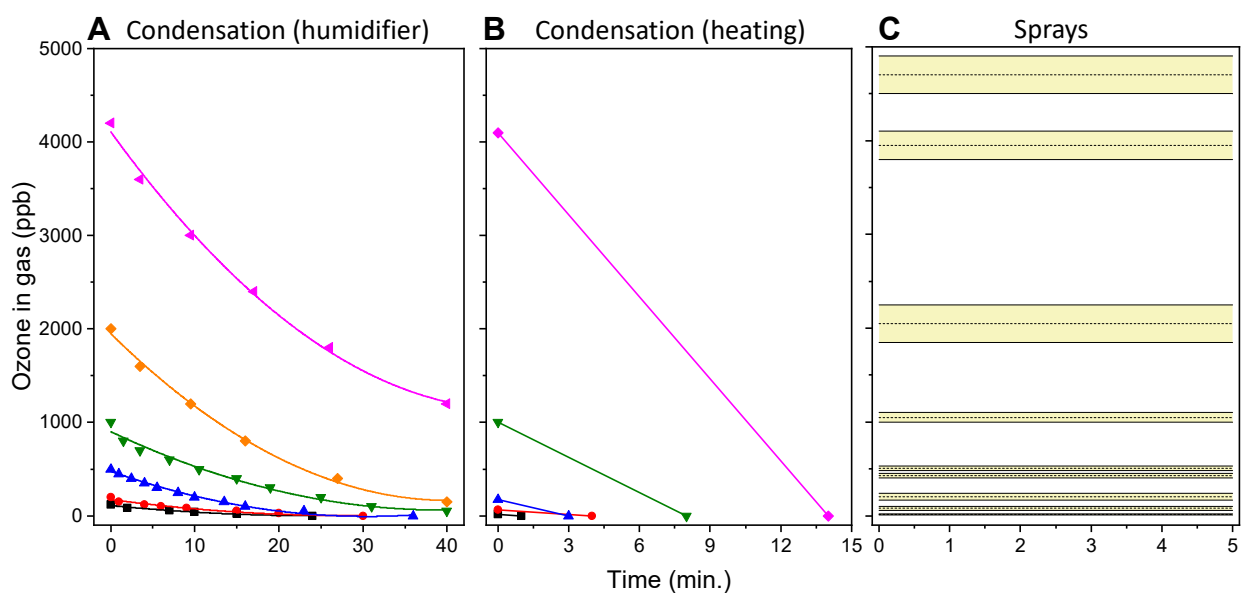


Fig. S8 – Gradual depletion of ozone from the glovebox for different initial ozone concentrations in (A) condensation by using the ultrasonic humidifier as the humidity source, and (B) condensation by heating water as the humidity source. (C) Range of ozone concentration for sprays showing no depletion. Ozone was added to the specified initial concentration in (A-B) while ozone was manually adjusted within the yellow bands (C) for the spray experiment.

Reaction with water combined with oxidation of elements inside of the glovebox (i.e., metal support, electrical outlet, etc.) and some leakage through the glovebox outlet contributed to the ozone depletion observed in Fig. S8A-B. We compared those effects by measuring depletion of ozone from the glovebox with and without water (Fig. S9); 120 mL of water was placed inside shallow containers with a surface area of 390 cm<sup>2</sup>. We observed that the O<sub>3</sub>(g) depletion in the presence of water was faster. From the difference in the ozone concentration at ~55 min, and with the glovebox volume of 140 L, we estimated that ~0.7 μmol of ozone diffused into the water; assuming a 1:1 ozone to H<sub>2</sub>O<sub>2</sub> molar conversion, the concentration of H<sub>2</sub>O<sub>2</sub> in the liquid was expected to be ~5.8 μM. From our experimental measurements, we obtained 0.85 μM, which is ~15% of the estimated value. Despite the difference, this indicates that ozone is indeed being converted to H<sub>2</sub>O<sub>2</sub>. The difference from the measured to the calculated values could be attributed to slightly different rates of ozone depletion in the glovebox, i.e., oxidation of its internal components, or to lower ozone to peroxide conversion ratios.

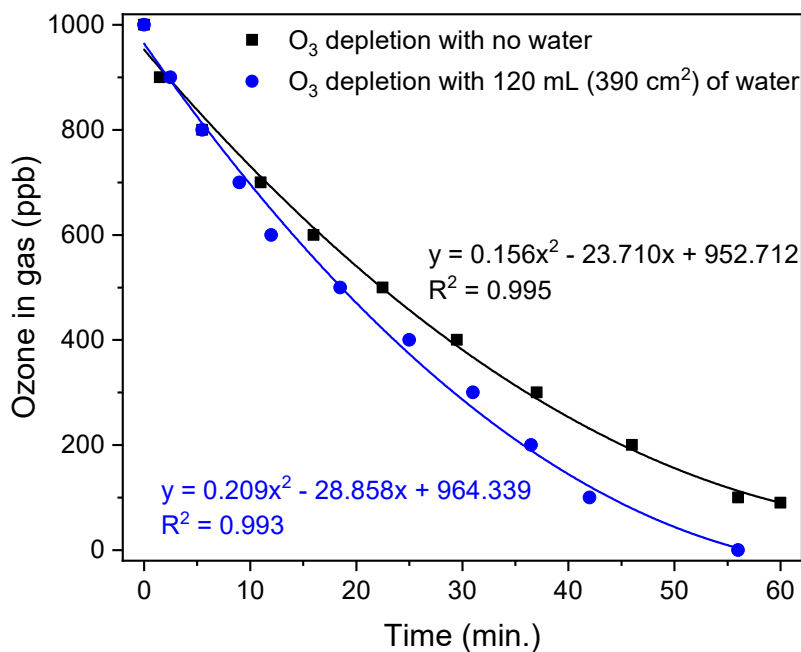


Fig. S9 – Gradual depletion of ozone from the glovebox with and without the presence of water at the same conditions.

## References

1. Muszkopf, N. H.; Gallo Jr, A.; Zhang, P.; Petry, J.; Mishra, H., The air-water interface of condensed water microdroplets does not produce H<sub>2</sub>O<sub>2</sub>. *J. Phys. Chem. Lett.* **2021**, *12*, 11422–11429.
2. Han, Z.; Reitz, R. D., Turbulence modeling of internal combustion engines using RNG  $\kappa$ - $\epsilon$  models. *Combustion Science and Technology* **1995**, *106* (4-6), 267-295.
3. Hirt, C. W.; Nichols, B. D., Volume of fluid (VOF) method for the dynamics of free boundaries. *Journal of computational physics* **1981**, *39* (1), 201-225.
4. Richards, K.; Senecal, P.; Pomraning, E. *CONVERGE (v3.0)*; Madison (WI): Convergent Science.
5. Kee, R. J.; Rupley, F. M.; Miller, J. A. *CHEMKIN II: A fortran chemical kinetics package for the analysis of gas-phase chemical kinetics*; Sandia National Laboratories, 1989.